Impact of Subarray Position Errors in mm-Wave MIMO Automotive Radar Polarimetric Phase Calibration

Changxu Zhao[1],Yanki Aslan[1], Alejandro Garcia-Tejero[2], and Alexander Yarovoy[1]
(1) Delft University of Technology, Delft, The Netherlands
(2) HUBER+SUHNER AG, Switzerland

Abstract

The impact of subarray position errors on polarimetric phase calibration in mm-wave MIMO automotive radar systems is studied for the first time. A $\pm 45^\circ$ linearly polarized 77 GHz radar with an asymmetric MIMO topology is employed for demonstration purpose. The study reveals that minor subarray position deviations, about 0.03λ on average among the virtual array elements, can significantly influence the calibrated polarimetric phase response when the target is located off-broadside. Experimental results show that accounting for realized subarray positions reduces the cross-polarized phase difference's standard deviation by about 54%. For co-polarized targets at 30° azimuth and 60° azimuth, the mean phase difference decreases by 90% on average. These findings highlight the critical importance of using accurate subarray position information for processing and achieving reliable polarimetric calibration.

1 Introduction

Polarimetric measurements, which enable the extraction of a target's polarimetric scattering matrix, have gained increasing attention in the automotive domain. These measurements have been applied to enhance target detection [1], [2], classification [3], [4], and vehicle self-localization [5]. Recent studies also highlight the potential of polarimetry for recognizing road surface conditions [6]. However, to fully recover the scattering matrix information, proper amplitude and phase calibration of polarimetric radar systems is essential.

Calibrating polarimetric radar systems has been a key focus across various fields. In weather radar applications, researchers have addressed geometric distortions of the polarimetric basis when targets deviate from the broadside direction. Correction matrix techniques were developed to compensate for basis distortions in H-V polarized cross-dipole elements [7]. In the automotive domain, calibration of 77 GHz MIMO polarimetric radar has become increasingly prominent. The isolated antenna calibration technique (IACT) was employed in [8] to address channel imbalance issues. To minimize the need for multiple reference targets, a single rotatable dihedral corner reflector was proposed as a calibration target [9]. Despite these advancements, most calibration techniques focus on broadside measurements and were done on the amplitude of the polarimetric scattering matrix and not on phase and off-broadside targets [8]. Until recently, the authors presented a method for polarimetric phase calibration [10]. In cases involving off-broadside measurements, the positioning of MIMO subarrays introduces additional phase shifts between virtual elements [10]. Subarray position errors, which can arise from radar design optimizations or manufacturing tolerances, can result in errors in the calibrated polarimetric phase response. The impact of such errors on the derived scattering matrix coefficients can be significant at mm-Wave. To the authors knowledge, the influence of MIMO subarray position errors on the polarimetric phase calibration has not yet been explored.

This paper addresses, for the first time, the influence of subarray position errors on off-broadside target's polarimetric phase calibration in mm-Wave MIMO automotive radar systems. A $\pm 45^\circ$ linearly polarized 77 GHz radar with an asymmetric MIMO topology is used for demonstration. The measurement results reveal the variations in calibrated polarimetric phase response under aimed and realized (after fabrication) subarray spacings. Off-broadside amplitude variations due to the polarimetric bias [7] is out of the scope of this paper.

The rest of the paper is organized as follows. The radar system and its layout are introduced in Section 2. The calibration method used in this research is discussed in Section 3. Section 4 discusses the measurement results. The paper is concluded in Section 5.

2 Radar antenna layout

This research utilizes a $\pm 45^\circ$ polarized MIMO automotive radar operating in the 77 GHz band, designed by HUBER+SUHNER AG. The radar measures the polarimetric scattering matrix, represented by Eq. (1). The MIMO topology and corresponding virtual array layout are illustrated in Fig. 1. The system includes four receivers, three transmitters, and a metalized plastic waveguide antenna manufactured using an innovative 3D printing technique developed by HUBER+SUHNER AG [11]. This antenna is mounted on the printed circuit board, as shown in Fig. 1a. The physical antenna channels are strategically positioned to achieve a fully populated virtual array with $\lambda/2$ spacing between the four polarimetric channels (S_{11}, S_{12}, S_{21}, S_{22}), as depicted in Fig. 1b.

$$S_{\pm 45^\circ basis} = \begin{bmatrix} S_{11} & S_{12} \\ S_{21} & S_{22} \end{bmatrix} = \begin{bmatrix} S_{+45+45} & S_{+45-45} \\ S_{-45+45} & S_{-45-45} \end{bmatrix} \quad (1)$$

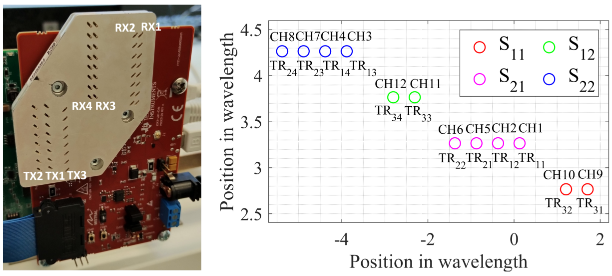

(a) MIMO topology layout **(b)** Polarimetric virtual array

Figure 1. Radar under test. [10]

The radar incorporates two subarray types, each offering orthogonal slant polarizations (±45°). These subarrays are based on a linear array of eight open waveguides [12]. Simulated radiation patterns for transmitter 1 and transmitter 3 are presented in Fig. 2. The subarrays achieve an elevation 3-dB field-of-view (FOV) of 9.1° and an azimuthal FOV of 105°. Additionally, cross-polarization isolation reaches 35 dB at boresight, decreasing to 5 dB at 60° in the azimuthal plane.

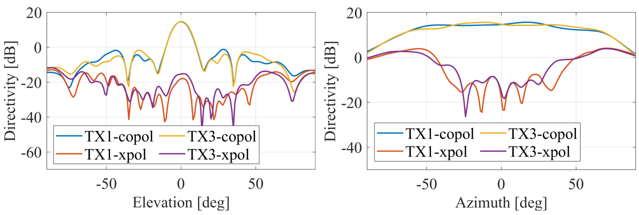

(a) phi=90° cut **(b)** phi=0° cut

Figure 2. TX1 (+45°) and TX3 (-45°) subarray simulated radiation pattern [10].

In this study, the target is assumed to be fixed at 0° in the elevation plane and measured in the far-field of the radar. Consequently, the separation of virtual elements along the vertical axis (shown in Fig. 1b) can be disregarded, as it does not introduce additional polarimetric phase shifts to the received signal. By aligning the virtual elements at the same elevation, the corresponding spacing between them is illustrated in Fig. 3, where $\lambda/2$ and λ are used as the reference spacings. However, due to manufacturing tolerances, the realized positions of the subarrays (listed in Table 1) slightly deviate from the aimed configuration. These deviations are shown in Fig. 4, where all virtual element spacings exhibit minor variations from the aimed $\lambda/2$ or λ values. The average deviation is approximately 0.032λ (0.12 mm). While these deviations appear small, they can cause significant changes in the polarimetric phase response of the channels when the target is measured off-broadside.

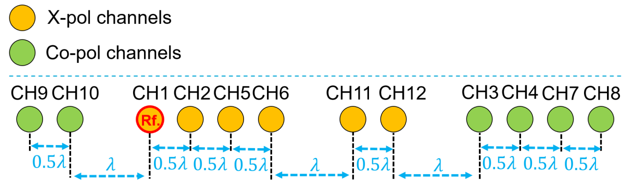

Figure 3. Virtual elements spacing (aimed), Rf. denotes the reference channel for additional phase shift compensation.

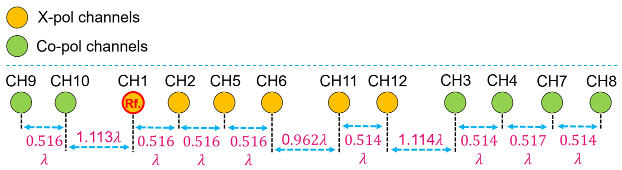

Figure 4. Virtual elements spacing (realized), Rf. denotes the reference channel for additional phase shift compensation.

Table 1. Location of the subarray physical centers.

	TX1	TX2	TX3	RX1	RX2	RX3	RX4
x-coordinate [mm]	-9.97	-16.16	-20.08	16.66	14.7	0.935	-1.02
y-coordinate [mm]	-6.34	-4.38	-4.38	17.18	17.18	21.1	21.1

3 Polarimetric phase calibration method

To accurately measure the polarimetric phase response of a target, this research adopts the calibration method proposed in [10]. A rotatable dihedral corner reflector is used as the calibration target due to its angular-dependent scattering properties, expressed in Eq. (2), where α represents the rotation angle and σ_{DH} denotes its radar cross section (RCS). For radar with ±45° polarization, the dihedral rotated to 0° is selected as the cross-polarization target, while the 45° rotated dihedral serves as the co-polarization target. The calibration matrix (C_{cal}) is derived by computing the ratio between the reference channels (channel 1 and channel 3 in this study) and the other channels, based on measurements from the dihedral [10]. A trihedral corner reflector, with its scattering matrix (S_{TH}) shown in Eq. (2) and σ_{TH} as its RCS, is employed as the validation target in this research.

$$S_{DH}(\alpha) = \sqrt{\frac{\sigma_{DH}}{4\pi}} \begin{bmatrix} -\cos 2\alpha & \sin 2\alpha \\ \sin 2\alpha & \cos 2\alpha \end{bmatrix} \quad S_{TH} = \sqrt{\frac{\sigma_{TH}}{4\pi}} \begin{bmatrix} 1 & 0 \\ 0 & 1 \end{bmatrix} \quad (2)$$

When the target is located off-broadside, additional phase shifts (Φ_{prog}) are introduced among the virtual elements based on the angle of arrival (AOA). This causes the polarimetric phase response of the channels to deviate from the theoretical scattering matrix of the target. The additional phase shifts on each virtual element (CH_i, where

$i = 1...12$) are calculated using Eq. (3), where d_i is the spacing between CH_i virtual element and the reference element (CH1), c is the speed of light, and f_c is the radar's operational frequency. To correct the phase shift, one channel is designated as the reference (channel 1 in this study), and the relative phase differences for the remaining channels are compensated accordingly. The spacing between virtual elements significantly influences the value of the phase shift. Any deviations in the spacing result in errors in the calculated phase shift, ultimately affecting the corrected polarimetric phase response.

$$\Phi_{prog_i} = sin\Phi_{AOA} \cdot \frac{d_i}{c} \cdot 2\pi f_c \quad (3)$$

4 Measurement results

The measurements were conducted in the anechoic chamber at TU Delft using a rotatable dihedral and a trihedral as targets. Both targets were larger than 10λ at 77 GHz, with a separation of 3.6 meters from the radar. During off-broadside measurements, the targets remained oriented towards the radar. Two stepper motors were employed to control the radar's azimuthal scanning and the dihedral's rotation angle. Fig. 5 shows the measurement setup in the anechoic chamber.

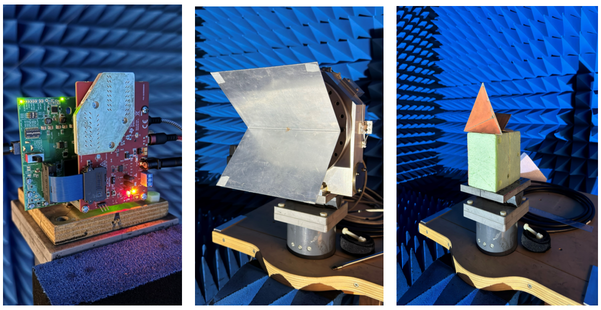

(a) Radar under test **(b)** Dihedral **(c)** Trihedral

Figure 5. Measurement setup in the anechoic chamber.

Following the measurements, the data was calibrated using the previously described method. To account for the impact of subarray positioning, progressive phase compensation was performed using both the aimed subarray positions (resulting in standard $\lambda/2$ and λ virtual element spacings) and the realized subarray positions. The results were evaluated by calculating the channels' polarimetric phase differences: the co-polarized channels' phase difference ($|\phi_{+45+45} - \phi_{-45-45}|$) and the cross-polarized channels' phase difference ($|\phi_{+45-45} - \phi_{-45+45}|$). A summary of the results, where s.t.d. stands for the standard deviation, is presented in Table 2. According to the scattering matrix of the dihedral rotated to 90°, when measured by a $\pm45°$ polarized radar, the polarimetric phase difference between cross-polarized channels should give zero in both mean and s.t.d. Similarly, the measured co-polarized channels phase difference from a trihedral should also give zero in both mean and s.t.d.

For validation a 90° rotated dihedral was used as the cross-polarized target. As shown in Fig. 6, accounting for the realized subarray position (Fig. 6b) to compensate for the additional phase shift reduced the standard deviation of the cross-polarized phase difference from 9.14° to 4.16°. After this adjustment, the polarimetric phase response of the cross-polarized channels became more consistent, aligning more closely with the theoretical expectation for a 90° rotated dihedral under $\pm45°$ polarized wave incidence, where the phase difference between cross-polarized channels is ideally zero.

Similarly, the trihedral corner reflector was employed as the co-polarized validation target, where the expected polarimetric phase difference between co-polarized channels is also zero. At a 30° azimuth angle (Fig. 7), the realized subarray position reduced the mean co-polarized phase difference from 58.13° to 8.44°, with a corresponding standard deviation reduction of 1.64°. At 60° azimuth (Fig. 8), the mean phase difference decreased by 86.16°, and the standard deviation dropped by 5.81°. In both cases, as shown in Fig. 7 and Fig. 8, using the realized subarray position (Fig. 7b, Fig. 8b) resulted in a more consistent polarimetric phase response of the co-polarized channels compared to using the aimed subarray position (Fig. 7a, Fig. 8a).

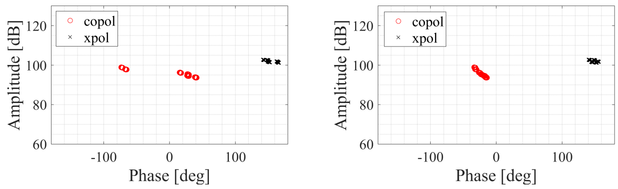

(a) **(b)**

Figure 6. Phase calibrated off-broadside measurement of the 90° rotated DH at 60° in azimuth using: (a) aimed subarray position, (b) realized subarray position.

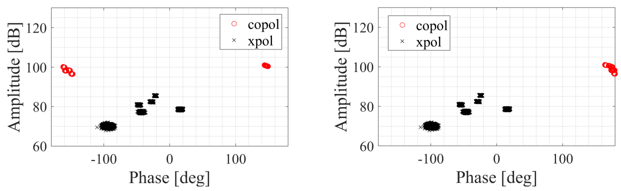

(a) **(b)**

Figure 7. Phase calibrated off-broadside measurement of the trihedral at 30° in azimuth using: (a) aimed subarray position, (b) realized subarray position.

Table 2. Off-broadside polarimetric phase calibration results.

	Aimed element spacing		Realized element spacing	
	$\lvert\phi_{+45-45} - \phi_{-45+45}\rvert$ [deg]			
	Mean	S.t.d	Mean	S.t.d
90° rotated DH, azi60°	-9.77	9.14	-6.9	4.16
	$\lvert\phi_{+45+45} - \phi_{-45-45}\rvert$ [deg]			
	Mean	S.t.d	Mean	S.t.d
TH, azi30°	58.13	5.36	8.44	3.72
TH, azi60°	92.87	9.57	6.71	3.76

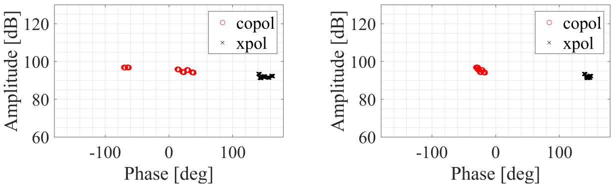

(a) **(b)**

Figure 8. Phase calibrated off-broadside measurement of the trihedral at 60° in azimuth using: (a) aimed subarray position, (b) realized subarray position.

5 Conclusion

This study examined the influence of subarray position errors on polarimetric phase calibration in mm-wave MIMO automotive radars for off-broadside measurements. Using a ±45° polarized 77 GHz radar with an asymmetric MIMO topology, it is demonstrated that slight deviations (around 0.03λ on average) from aimed subarray positions significantly impact the calibrated polarimetric phase response. For the cross-polarized target, compensating for realized subarray positions reduced the s.t.d. of the phase difference from 9.14° to 4.16°. Similarly, for the co-polarized target, the measurements from the trihedral at 30° and 60° in the azimuth plane show the mean phase difference drops significantly for about 90% on average after using the realized subarray position. These results underscore the critical role of subarray position accuracy in achieving reliable polarimetric calibration in off-broadside measurement and provide valuable insights into the design and calibration of polarimetric MIMO radars.

6 Acknowledgements

This research was supported by the National Growth Fund through the Dutch 6G flagship project "Future Network Services". I would like to extend my heartfelt gratitude to Wietse Bouwmeester for his invaluable contributions to the setup of the polarimetric radar system, which was instrumental in this research. Special thanks go to Pascal Aubry for his exceptional support in establishing the measurement environment and assisting with the measurements.

References

[1] T. Visentin, J. Hasch, and T. Zwick, "Analysis of multipath and DOA detection using a fully polarimetric automotive radar," in *2017 European Radar Conference (EURAD)*, Oct. 2017, pp. 45–48.

[2] J. F. Tilly, F. Weishaupt, O. Schumann, J. Dickmann, and G. Wanielik, "Road User Detection on Polarimetric Pre-CFAR Radar Data Level," *IEEE Robotics and Automation Letters*, vol. 8, no. 6, pp. 3558–3565, Jun. 2023, Conference Name: IEEE Robotics and Automation Letters.

[3] J. F. Tilly, O. Schumann, F. Weishaupt, J. Dickmann, and G. Waniliek, "Polarimetric Information Representation for Radar based Road User Detection with Deep Learning," in *2021 IEEE 24th International Conference on Information Fusion (FUSION)*, Nov. 2021, pp. 1–6.

[4] J. F. Tilly, F. Weishaupt, O. Schumann, J. Dickmann, and G. Wanielik, "Road User Classification with Polarimetric Radars," in *2020 17th European Radar Conference (EuRAD)*, Jan. 2021, pp. 112–115.

[5] F. Weishaupt, J. F. Tilly, J. Dickmann, and D. Heberling, "Polarimetric Covariance Gridmaps for Automotive Self-Localization," in *2020 IEEE 23rd International Conference on Information Fusion (FUSION)*, Jul. 2020, pp. 1–8.

[6] W. Bouwmeester, F. Fioranelli, and A. G. Yarovoy, "Road surface conditions identification via h α a decomposition and its application to mm-wave automotive radar," *IEEE Transactions on Radar Systems*, vol. 1, pp. 132–145, 2023.

[7] G. Zhang, *Weather Radar Polarimetry*. Taylor & Francis Group, May 2016.

[8] T. Visentin, J. Hasch, and T. Zwick, "Calibration of a fully polarimetric 8×8 mimo fmcw radar system at 77 ghz," in *2017 11th European Conference on Antennas and Propagation (EUCAP)*, Mar. 2017, pp. 2530–2534.

[9] A. Tinti, S. Tejero Alfageme, S. Duque Biarge, J. Balcells-Ventura, and N. Pohl, "Fully Polarimetric Automotive Radar: Proof of Concept," *IEEE Transactions on Radar Systems*, vol. 2, pp. 645–660, 2024, ISSN: 2832-7357.

[10] C. Zhao, A. Garcia-Tejero, W. Bouwmeester, Y. Aslan, O. Krasnov, and A. Yarovoy, "Calibration of Polarimetric Automotive Radar With Asymmetric MIMO Topology and Off-Broadside Beamforming," in *2024 21st European Radar Conference (EuRAD)*, Sep. 2024, pp. 87–90.

[11] U. Huegel, A. Garcia-Tejero, R. Glogowski, E. Willmann, M. Pieper, and F. Merli, "3D waveguide metallized plastic antennas aim to revolutionize automotive radar.," *Microwave Journal*, vol. 65, no. 9, 2022.

[12] A. Garcia-Tejero, M. Burgos-Garcia, and F. Merli, "High-efficiency injection-molded waveguide horn antenna array for 76-81 ghz automotive radar applications," in *2022 19th European Radar Conference (EuRAD)*, 2022, pp. 21–24.